Catalysis Today 169 (2011) 60–68

Contents lists available at ScienceDirect

Catalysis Today

journal homepage: www.elsevier.com/locate/cattod

Genesis of active and inactive species during the preparation of MoO_3/SiO_2–Al_2O_3 metathesis catalysts via wet impregnation

Damien P. Debecker[a,*], Mariana Stoyanova[b], Uwe Rodemerck[b], Alexandre Léonard[c], Bao-Lian Su[c], Eric M. Gaigneaux[a]

[a] Institute of Condensed Matter and Nanoscience - MOlecules, Solids and reactiviTy (IMCN/MOST), Université catholique de Louvain, Croix du Sud 2/17, 1348 Louvain-La-Neuve, Belgium[1]
[b] Leibniz-Institut für Katalyse e.V. an der Universität Rostock, Albert-Einstein-Str. 29a, 18059 Rostock, Germany
[c] Laboratoire de Chimie des Matériaux Inorganiques (CMI), Facultés Universitaires Notre-Dame de la Paix (FUNDP), 61 rue de Bruxelles, B-5000 Namur, Belgium

ARTICLE INFO

Article history:
Available online 15 September 2010

Keywords:
Propylene metathesis
Anderson heteropolyanion
Mesoporous mixed oxide
Sintering
Dispersion
Aluminium molybdate
AHM

ABSTRACT

The wet impregnation of ammonium heptamolybdate onto silica–alumina is used to prepare MoO_3/SiO_2–Al_2O_3 heterogeneous metathesis catalysts. The preparation is inspected in details in conjunction with physico-chemical characterization tools with the aim to identify the parameters that dictate the genesis of active and inactive metathesis species. The effects of the MoO_3 loading and of the calcination temperature are systematically explored. The samples are characterized by N_2-physisorption, ICP-AES, XRD, Raman, ^{27}Al MAS-NMR and XPS and evaluated in the metathesis of propene to butene and ethene. Particular attention is brought to the interaction of the mesoporous silica–alumina support with the active component, to the decomposition of the precursor salt and to the location of the molybdenum oxide phase with respect to the pores of the support. It is shown that the temperature of calcination influences markedly the performances of the catalyst. High temperature treatments are necessary to decompose efficiently the Mo salt precursor. In the metathesis of propylene, the performances are levelling off when the MoO_3 loading is increased above ~8 wt.%. This effect is correlated to the build up of MoO_3 crystals and of $Al_2(MoO_4)_3$ at relatively high loading.

1. Introduction

The most convenient way to prepare a MoO_3-based catalyst is to impregnate a Mo precursor on the dedicated support and to decompose this precursor to Mo oxide via thermal treatment. The wet impregnation of ammonium heptamolybdate (AHM) on silica, alumina or silica–alumina supports is commonly used for the preparation of MoO_3-based metathesis catalysts [1,2]. The details of the preparation method impact markedly on essential properties of the final catalytic material: morphology of the MoO_3 deposit, nature and proportion of Mo oxide species, interaction of Mo atoms with the support, etc. In turn, these properties are seen as crucial parameters that dictate the performance of the catalyst. However, the intricate relationships between (i) the preparation parameters, (ii) the catalysts properties and (iii) the metathesis activity remain unclear. It is widely accepted for example that well-dispersed MoO_x species, as opposed to MoO_3 crystals, are the precursors for active sites. Nevertheless, a debate still persists on their nature (monomeric [3], dimeric [4], polymeric [5]). Similarly, the nature of the support was shown to have a marked impact on the catalytic activity [6,7] and intimate interaction between the active phase and support are often sought for. However, strong interactions leading to the formation of mixed phases is suggested to be deleterious (e.g. aluminium molybdate [8]). It should be reminded also that only a small proportion of Mo atoms in supported MoO_3 catalysts turn out to be active in the metathesis reaction [9]. As diffraction or spectroscopic methods mainly depict the majority sites, it often remains difficult to correlate characterization data with activity results. Computational methods are the only way to investigate surface sites that are in minority [10], but these theoretical approaches rely on simplified models presumably far away from the intricate situation encountered in silica–alumina-supported MoO_3-based catalysts. Overall, even if the wet impregnation route is rather classical, obtaining further experimental insights on the chemistry of these systems and on the formation of active and inactive Mo species is essential in the perspective of performance improvements.

This contribution proposes to study the preparation in a systematic way and to describe the Mo species at different stages

* Corresponding author. Tel.: +32 10473665; fax: +32 10473649.
E-mail addresses: damien.debecker@uclouvain.be (D.P. Debecker), eric.gaigneaux@uclouvain.be (E.M. Gaigneaux).
[1] *Note*: IMCN and MOST are new research entities involving the group formerly known as "Unité de catalyse et chimie des matériaux divisés".

0920-5861/$ – see front matter © 2010 Elsevier B.V. All rights reserved.
doi:10.1016/j.cattod.2010.07.026

of the catalyst preparation: impregnation solution, dried catalyst, calcined catalyst. These observations will be used to interpret the catalytic behaviour of the catalysts in the self-metathesis of propene. Most parameters of the preparation were carefully kept constant (volume of impregnation solution, amount of support, stirring, impregnation time, drying time, calcination time, etc.). The support used is a commercial mesoporous silica–alumina with a composition (13 wt.% of Al_2O_3) very close to the optimum composition determined in a recent study [6]. Two important parameters of the preparation were systematically varied: the calcination temperature and the nominal molybdenum loading. The effects of these parameters on the physico-chemical properties of the catalysts are followed by characterizing them via N_2-physisorption, inductively coupled plasma-atomic emission spectroscopy (ICP-AES), X-ray diffraction (XRD), X-ray photoelectron spectroscopy (XPS), magic angle spinning-nuclear magnetic resonance (MAS-NMR) and Raman spectroscopy.

The nominal Mo loading and the calcination temperature were studied for their potential impact on the final performance of the yielded metathesis catalysts. The calcination of the catalyst leads to the decomposition of the ammonium heptamolybdate salt and to the formation of a Mo oxide phase. Changing the calcination temperature may affect the efficiency of this step (well-formed Mo oxide vs. partially decomposed molybdenum salt). Also, the strength of the thermal treatment may affect the dispersion of the Mo phase. On the one hand, high temperature treatments are known to favour sintering phenomena, potentially leading to the formation of MoO_3 crystals. On the other hand, MoO_3 is known to be quite volatile and harsh thermal treatment might also promote the dispersion of Mo on the support [11,12] or provoke Mo losses.

Molybdenum oxide is the active component of the catalyst and its loading is evidently crucial. In principle, the amount of active centres could be partially linked to the amount of Mo introduced in the formulation. In the case of MoO_3-based metathesis catalysts however, studies show that there is no direct relationship between catalytic activity and MoO_3 loading [13]. Very often, the activity increases with the increase in the MoO_3 loading only up to a given loading. Then the performances level off or decrease sharply [7,14–16]. Changing the nominal loading induces a change in the AHM concentration in the fixed impregnation solution volume. Also, as the available surface area of the support remains constant, the Mo surface density in the resulting catalyst varies. In turn, the mode of dispersion of Mo oxide can be affected as well as the nature of the Mo species stabilized on the support.

The purpose of the study is to show how the preparation parameters impact on the genesis of given Mo species during the preparation and in the final catalytic material. Particular attention is devoted to the interaction of the support with the active component, to the decomposition of the precursor salt, to the nature of the generated Mo species and to their location with respect to the porosity of the silica–alumina support. These observations are then exploited in the interpretation of the behaviour of the catalysts in the metathesis reaction.

2. Experimental methods

2.1. Catalyst preparation

The catalysts are prepared by wet impregnation of ammonium heptamolybdate (AHM) on a commercial silica–alumina (Aldrich, Grade 135). The support contains ca. 13 wt.% of Al_2O_3 and has a specific surface area of 490 $m^2\ g^{-1}$. Prior to impregnation, the support is calcined at 500 °C for 15 h under static air. An initial precursor solution was prepared by dissolution of 12.268 g of AHM in distilled water (6.66 g of Mo per l). $(NH_4)_6Mo_7O_{24}{\cdot}H_2O$ was purchased from Aldrich and had a purity of 99.98%. An appropriate amount of this precursor solution (depending on the nominal MoO_3 loading targeted for each synthesis) was diluted in distilled water to yield a 200 ml impregnation solution. 4 g of calcined support was then suspended in the impregnation solution for 2 h under magnetic stirring. Water was then evaporated under reduced pressure in a rotavapor at 40 °C. The recovered solid was dried at 110 °C for one night and calcined for 2 h in a muffle furnace under static air. The samples are denoted AA*xY*, where the first 'A' stands for the Aldrich support, the second 'A' stands for the AHM precursor, *x* is the nominal MoO_3 weight loading (%) and *Y* is the calcination temperature (°C). First, the loading (*x*) is fixed at 8 wt.% (following typical values proposed in the literature [17–19]) and the effect of calcination is followed (*Y* = 300, 400 and 500 °C). Then, the best calcination temperature is selected and the MoO_3 loading is screened in the 4–16 wt.% range.

2.2. Catalyst characterization

The weight percentages of Mo, Si and Al were measured by inductively coupled plasma-atomic emission spectroscopy (ICP-AES) on an Iris Advantage apparatus from Jarrell Ash Corporation. The materials were dried at 105 °C prior to measurements.

N_2-physisorption experiments were performed at −196 °C on a Micromeritics Tristar. The samples were outgassed at 150 °C under vacuum (2 Pa). The specific surface area was determined from the BET method in 0.05–0.30 P/P_0 range. The pore size distribution was derived from the desorption branch using the BJH method. The average pore diameter is calculated as (4 × pore volume/BET specific surface area).

X-ray diffraction (XRD) measurements were performed with a Siemens D5000 diffractometer using the Kα radiation of Cu (λ = 1.5418 Å). The 2θ range was recorded between 5° and 75° at a rate of 0.02° s^{-1}. The ICDD–JCPDS database was used to identify the crystalline phases.

Confocal Raman spectroscopy was done on the InVia Raman microscope (Renishaw) equipped with a diode light (785 nm). The resolution was set to 4 cm^{-1}. Acquisition time was 10 s and 10 scans were recorded and averaged for each catalyst. The laser power was set to 10 mW and the 50× objective was used. The precursor solution was analyzed via Fourier transform Raman spectroscopy (FT-Raman) with the Bruker RFS 100/S apparatus. About 1 ml of the solution was introduced in a dedicated quartz cell. A coherent Nd-YAG laser of 1064 nm wavelength was used and its power was set to 450 mW. The resolution was 4 cm^{-1} and the frequency was analyzed in the 1600–100 cm^{-1} range. For each reported spectra 720 scans were recorded and averaged.

X-ray photoelectron spectroscopy (XPS) was performed on a Kratos Axis Ultra spectrometer (Kratos Analytical – Manchester – UK) equipped with a monochromatized aluminum X-ray source (powered at 10 mA and 15 kV). The pressure in the analysis chamber was about 10^{-6} Pa. The analyzed area was 700 μm × 300 μm. The pass energy of the hemispherical analyzer was set at 160 eV for the wide scan and 40 eV for narrow scans. Charge stabilization was achieved by using the Kratos Axis device. The electron source was operated at 1.8 A filament current and a bias of −1.1 eV. The charge balance plate was set at −2.8 V. The sample powders were pressed into small stainless steel troughs mounted on a multi specimen holder. The following sequence of spectra was recorded: survey spectrum, C 1s, O 1s, Si 2p, Al 2p, Mo 3d, Mo 3p & N 1s and C 1s again to check for charge stability as a function of time and for the absence of degradation of the sample during the analyses. The binding energy (BE) values were referred to the C–(C, H) contribution of the C 1s peak fixed at 284.8 eV. Molar fractions (%) were calculated using peak areas normalized on the basis of acquisition parameters after a linear background subtraction, with experimental sensitiv-

ity factors and transmission factors provided by the manufacturer. Spectra were decomposed with the CasaXPS program (Casa Software Ltd., UK) with a Gaussian/Lorentzian (70/30) product function.

The Bruker Avance 500 apparatus was used to record the magic angle spinning-nuclear magnetic resonance (MAS-NMR) of ^{27}Al, using a flip of 10° (with respect to the vertical) and recording 5000 scans for each sample at intervals of 0.1 s. The sample rotation speed was 15,000 rpm.

2.3. Propene metathesis

The evaluation of the metathesis activity of the catalysts was carried out in a multi-channel apparatus with a capacity of treating of up to 15 samples under identical conditions [20]. The whole design allows fully automated control of gas flows and of 3 temperature zones (gas pre-heating, reactor, and post reactor lines with 16-port valve) along with reactor switching and product sampling. All catalysts were sieved and selected in the 200–315 μm granulometric size range. The catalysts (200 mg) were introduced in quartz straight reactors (5 mm i.d.). In each experiment, several samples were pre-treated in parallel by heating up to 550 °C (temperature ramp of 5 °C min^{-1}) in N_2 (14 ml min^{-1} flow in each reactor) and keeping this temperature for 2 h. Afterwards the system was cooled down to the reaction temperature (40 °C) under the same N_2 flow. A propene (99.95% purity) flow of 8 ml min^{-1} was admitted for 1 h sequentially in each reactor in order to measure the initial metathesis activity of each sample. During activity measurement, the other reactors are kept under the same N_2 flow. Propene and nitrogen were purified over Molsieve 3A (Roth) filters. N_2 was also purified by an oxygen filter (Oxysorb-glass, Linde). The composition of the reaction gas was analyzed by an Agilent 6890 GC. Product analysis took about 6.5 min for each injection. The separation of hydrocarbons was performed on a HP-AL/M column (30 m length, 0.53 mm i.d., 0.15 μm film thickness) applying a temperature ramp between 90 and 140 °C and FID detection. The experiments were carried out at atmospheric pressure.

The selectivity to metathesis products was always found to be very close to 100% (typically 99%). Only traces of secondary metathesis products (1-butene, pentenes, hexenes) and isomerization products (isobutene) were detected. The activity is calculated on the basis of metathesis products (ethene and *trans*- and *cis*-butene) formation. The specific activity is defined as the number of moles of propene converted to metathesis products per gram of catalyst and per hour. The standard deviation for activity measurements is less than 3% in relative.

3. Results

3.1. Catalysts preparation and characterization

The initial precursor solution (6.66 g of Mo per l) was obtained by dissolution of ammonium heptamolybdate in distilled water. In Raman spectroscopy (Fig. 1), this solution exhibited two main bands at 942 and 895 cm^{-1} that are attributed to the presence of the heptamolybdate ions (respectively the ν_s MoO_{2t} and the ν_{as} MoO_{2t} vibrations) [21,22]. The pH of this solution was 5.4. The desired volume of this solution (depending on the targeted MoO_3 loading) was diluted in water and used for impregnation of the support.

The experimental MoO_3 weight loading and the textural properties of the catalysts are given in Table 1. The experimental loading fits with the nominal composition of the samples. All samples were mesoporous, with N_2 adsorption–desorption isotherms of type IV according to the IUPAC classification. Such isotherms are shown in Fig. 2 in the case of the bare support taken as a representative example for all investigated catalysts. The calcination temperature

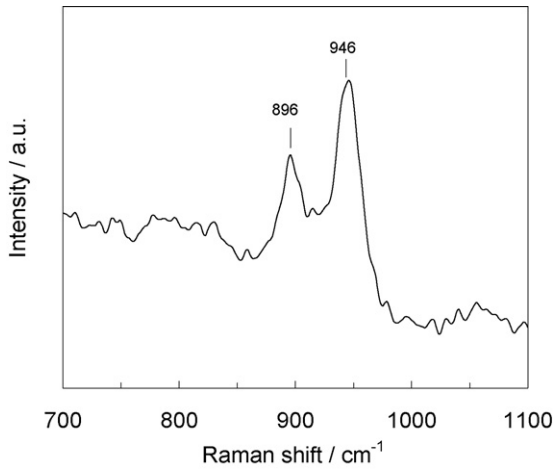

Fig. 1. FT-Raman spectrum of the initial AHM precursor solution used for the preparation of the catalysts.

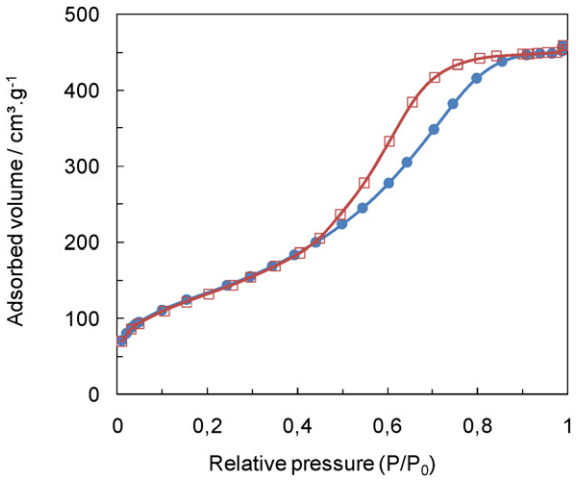

Fig. 2. N_2 adsorption (●) and desorption (□) isotherms at −196 °C for the silica–alumina support ("A").

has no significant effect on the specific surface area of the 8% loaded samples. When the calcination temperature is fixed at 500 °C, the specific area and the pore volume clearly tend to decrease with increasing MoO_3 loading. On the other hand, the average pore diameter in the catalysts is equal to that of the bare support or slightly higher.

Figs. 3 and 4 were drawn in order to better visualize the effect of the MoO_3 loading and of the calcination temperature on the texture of the catalysts. After impregnation, the shape of the pore size distribution curve is unaffected and the whole curves shift downwards (following the ordinate axis) with each loading increment (Fig. 3). In fact these shifts are due to the addition of increasing

Table 1
Experimental MoO_3 weight loading (ICP-AES) and textural properties (N_2-physisorption).

Catalyst name	Exp. MoO_3 (wt.%)	SSA (m^2 g^{-1})	Pore volume (cm^3 g^{-1})	Average pore diameter (nm)
A	–	490	0.71	5.8
AA4500	3.8	440	0.63	5.7
AA8300	7.9	420	0.60	5.7
AA8400	8.3	400	0.57	5.7
AA8500	8.1	420	0.60	5.7
AA11500	10.9	380	0.55	5.8
AA16500	15.2	350	0.52	5.9

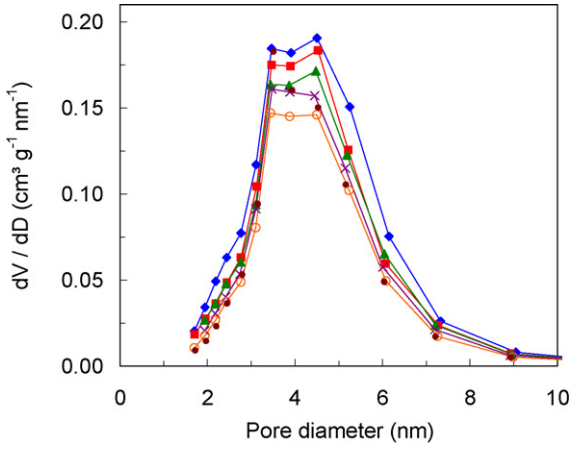

Fig. 3. Pore size distribution of: (♦) the support; (■) AA4500; (▲) AA8500; (×) AA11500; (○) AA16500.

amounts of MoO_3 which is non-porous. If the curves are normalized by the mass of support instead of the total mass of the sample, no significant alteration of the pore size distribution is observed. In the same way, the shape of the pore size distribution curves is not affected by changes in the calcination temperatures (Fig. 4).

XRD reveals the presence of a broad band (15–30°) typical of amorphous samples. In addition, diffraction lines related to the presence of MoO_3 crystals are detected in some cases. At 8% nominal weight loading, MoO_3 crystals tend to form if the calcination temperature is high (Fig. 5). More precisely, after calcination at 300 °C no crystallites are detected in XRD; small diffraction lines corresponding to traces of crystalline MoO_3 are distinguished on the catalyst calcined at 400 °C; these lines are much more pronounced after calcination at 500 °C (JCPDS 05-0508). In the catalysts calcined at 500 °C (Fig. 6), the diffraction lines related to orthorhombic MoO_3 grow in intensity as the loading increases. Only the AA4500 sample appears amorphous. The average size of the crystals detected in samples AA8500, AA11500 and AA16500 was estimated via the Debye–Scherrer law to fall in the 35–40 nm range.

Raman spectroscopy was also tentatively used to identify the nature of Mo oxide species present in the catalysts (Fig. 7). The support itself was found to give a strong background signal, most probably due to fluorescence created by defects and impurities in the support. AA*xY* samples were found to be quite heterogeneous in terms of Mo species detected by Raman spectroscopy. More precisely, spectra recorded on different particles of the same sample do

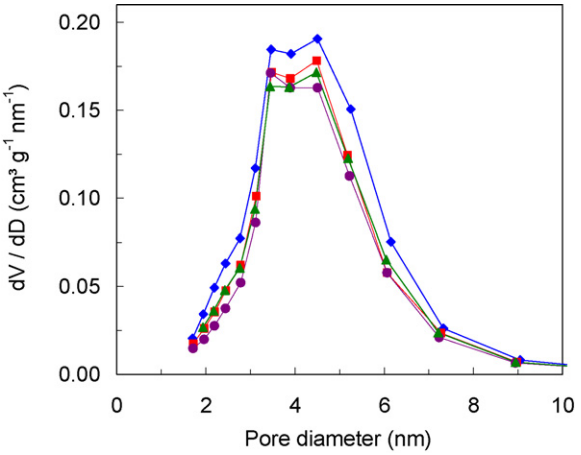

Fig. 4. Pore size distribution of: (♦) the support; (■) AA8300; (●) AA8400; (▲) AA8500.

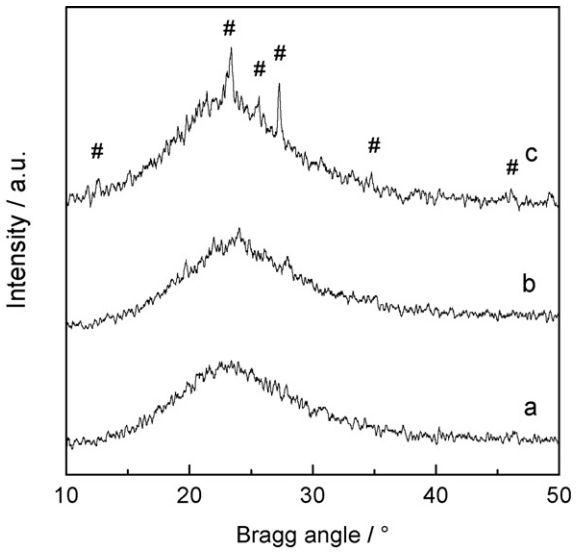

Fig. 5. XRD patterns of: (a) AA8300; (b) AA8400; (c) AA8500. # Symbols indicate the diffraction lines of orthorhombic MoO_3 (JCPDS 05-0508).

not reveal the same species. This indicates that the different species found in these samples are not evenly dispersed on all particles. Some spectra (Fig. 7, curve d) exhibit only a broad band around ca. 950 cm^{-1}. This signal is attributed to surface polymolybdates [22]. In other spectra (Fig. 7, curves b and c), sharper lines at 995 and 819 cm^{-1} were also detected, as clear evidence of the presence of MoO_3 crystals [22]. In fact, the latter signals were only detected on samples that yielded MoO_3 diffraction patterns in XRD. The main conclusion that can be drawn from these experiments, is that Raman spectroscopy confirms XRD analysis: signals related to the presence of MoO_3 crystals were only detected on the catalysts calcined at relatively high temperature (AA8400 and AA8500) and on catalysts with relatively high loading (AA11500 and AA16500), but never on the other samples.

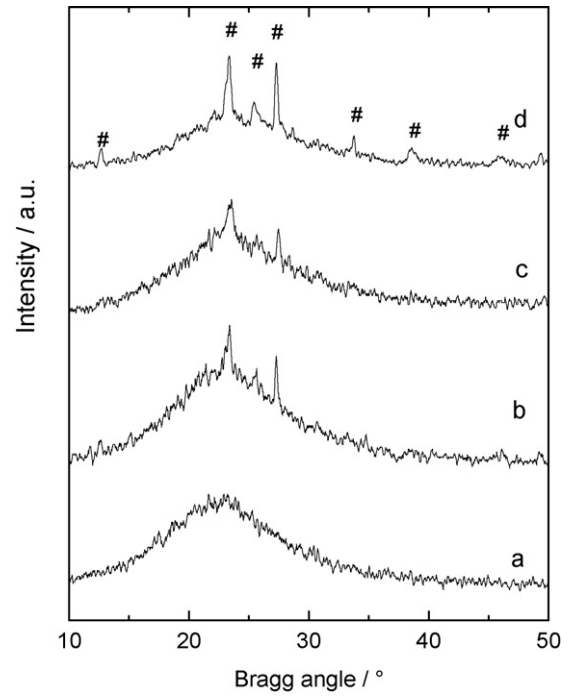

Fig. 6. XRD patterns of: (a) AA4500; (b) AA8500; (c) AA11500; (d) AA16500. # Symbols indicate the diffraction lines of orthorhombic MoO_3 (JCPDS 05-0508).

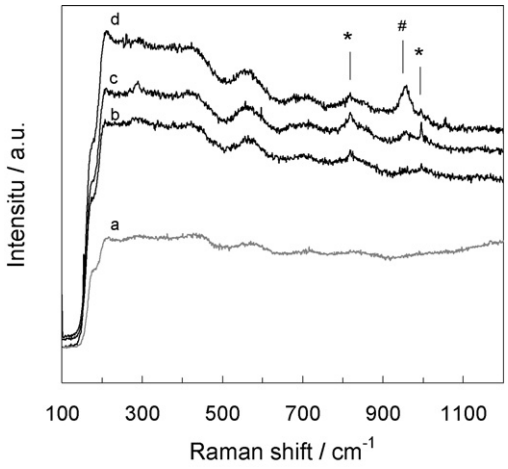

Fig. 7. Raman spectra of: (a) the support and of the AA8500 sample at 3 different positions (noted b, c and d) on the sample. More precisely, the same sample mounted under the microscope was analyzed 3 times, focusing the analysis on 3 distinct particles of solid. The "*" marks indicate the Raman signals of MoO_3 crystals and the "#" mark indicate the broad band related to polymolybdates.

The ^{27}Al MAS-NMR spectrum of the bare support is composed of three bands around 2, 30 and 54 ppm (Fig. 8). This spectrum closely resembles the one reported by May et al. [23] concerning a silica–alumina prepared by the sol–gel method with aluminum isopropoxide and tetraethoxysilane as precursors (13 wt.% Al_2O_3). The signal around 54 ppm is attributed to tetrahedrally coordinated framework Al atoms (Al_{TET}) typically found in silico-aluminic materials [24]. This coordination corresponds to Al atoms isomorphously substituting Si^{4+} in silica [25,26] or to a "transition alumina phase" that may form following segregation of phases during the preparation (and singularly during calcination) [27]. It is often referred to as the "framework tetrahedral species" [28]. The signal at about 2 ppm corresponds to Al octahedrally coordinated (Al_{OCT}). It is attributed either to γ-Al_2O_3 [27] or to an amorphous polymeric aluminium oxide phase [29]. The intermediate band at 30 ppm is often contradictorily attributed to distorted tetrahedral Al shifted by a strong quadrupolar interaction [30] or to 5-fold coordinated Al species

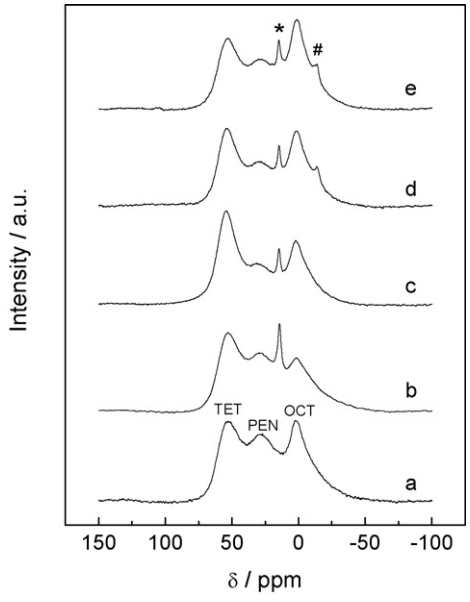

Fig. 8. ^{27}Al MAS-NMR spectra of: (a) the support; (b) AA8 uncalcined; (c) AA8300; (d) AA8400; (e) AA8500. The Al_{TET}, Al_{PEN} and Al_{OCT} broad signals are indicated on the first spectrum. [$AlMo_6$] and $Al_2(MoO_4)_3$ are marked with "*" and "#", respectively.

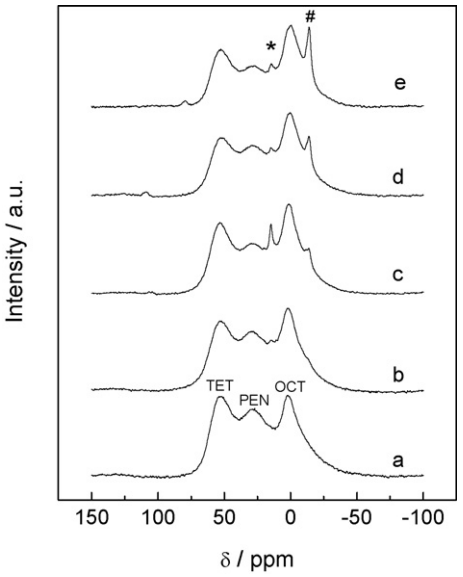

Fig. 9. ^{27}Al MAS-NMR spectra of: (a) the support; (b) AA4500; (c) AA8500; (d) AA11500; (e) AA16500. The Al_{TET}, Al_{PEN} and Al_{OCT} broad signals are indicated on the first spectrum. [$AlMo_6$] and $Al_2(MoO_4)_3$ are marked with "*" and "#", respectively.

(Al_{PEN}) [31–33]. Recent studies on amorphous silica–alumina systems and based on multiple quantum MAS-NMR measurements (that can distinguish between these two coordination states by separating the quadrupolar and chemical effects on the chemical shifts) unambiguously showed that this signal is attributable to five-coordinated Al atoms [24,28]. In silica–alumina, this coordination was assigned to the interface between an alumina-type phase and a truly mixed silica–alumina phase [34].

The introduction of Mo by wet impregnation of AHM modifies the ^{27}Al MAS-NMR fingerprint of the fresh support. In the uncalcined catalyst the Al_{OCT} component is significantly reduced. The Al_{PEN} signal also decreases slightly in intensity. Additionally, one sharp signal arises at 15 ppm. Several authors attribute this band to a hydrated form of $Al_2(MoO_4)_3$ [8] while others attribute it to the Anderson-type heteropolyanion $[Al(OH)_6Mo_6O_{18}]^{3-}$ [35,36] (vide infra). The calcination step again perturbs the ^{27}Al MAS-NMR spectra of the samples. The signal at 15 ppm decreases and, when the calcination temperature is 400 °C or higher, a peak at −14 ppm appears, which is broadly accepted to account for $Al_2(MoO_4)_3$ (non-hydrated) [8]. The Al_{OCT} contribution (at ca. 2 ppm) increases back after calcination. The intensity of this signal increases with the calcination temperature. Finally, let us note that the intensity of the signal at 15 ppm does not depend on the calcination temperature.

When the calcination temperature is kept at 500 °C and the MoO_3 loading is varied, the proportions of Al_{TET}, Al_{OCT} and Al_{PEN} do not change noticeably (Fig. 9). On the other hand the intensity of the signals due to the aluminium molybdate (at −14 ppm) phase increases obviously. This phase is barely detected at 4% wt. loading but clearly increases at higher loading. The peak at 15 ppm is always present.

The amount of Mo detected at the surface of the catalyst in XPS is obviously dependant on the loading: for the series of catalysts calcined at 500 °C a linear relationship is observed between the weight loading and the Mo/(Si + Al) XPS atomic ratio. Interestingly, the calcination temperature also has a drastic effect (Fig. 10). In particular, catalysts calcined at higher temperature exhibit a more intense superficial Mo signal. Note that all samples presented a well-defined Mo 3d doublet directly attributable to Mo^{VI} species.

For the series of samples with 8% MoO_3 weight loading and calcined at different temperatures a window of the XPS spectra around 400 eV has been recorded specifically to track the presence of nitro-

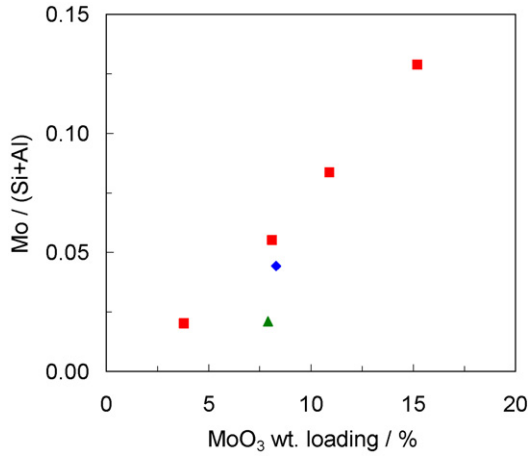

Fig. 10. Mo/(Si + Al) XPS atomic ratio for: (▲) AA8300; (♦) AA8400; (■) AA*x*500.

gen (Fig. 11). In this range of binding energies, the N 1s peak falls close to the Mo $3p_{3/2}$ peak. It was found that nitrogen – originating from the ammonium heptamolybdate precursor – is still detected on these calcined catalysts. This is particularly true for the catalyst calcined at lower temperature. Visibly, the intensity of the N 1s peak decreases with increasing temperature. In ammonium heptamolybdate ($(NH_4)_6Mo_7O_{24}{\cdot}H_2O$) there are 6 atoms of nitrogen for 7 atoms of Mo, meaning that the expected N/Mo atomic ratio is 0.86. Experimentally, a ratio of 0.82 was found by analyzing pure AHM in XPS. The same ratio calculated from the quantification of N and Mo in the AA8 samples equals 1.24, 0.79 and 0.25, respectively for AA8300, AA8400 and AA8500. For the AA8 sample before calcination (only dried), this ratio was measured to be 1.79. In other words, the wet impregnation clearly tends to provoke a relative increase in the proportion of N at the surface of the catalyst and the calcination temperature has a marked impact on the removal of the ammonium species.

3.2. Activity measurements

The evolution of the specific activity of the catalysts with time-on-stream (see supporting information) is similar as already reported for similar catalysts tested in the same reactor [6]. All catalysts exhibited a short latency stage followed by a maximum of activity after about 20 min. Then, as broadly observed and studied

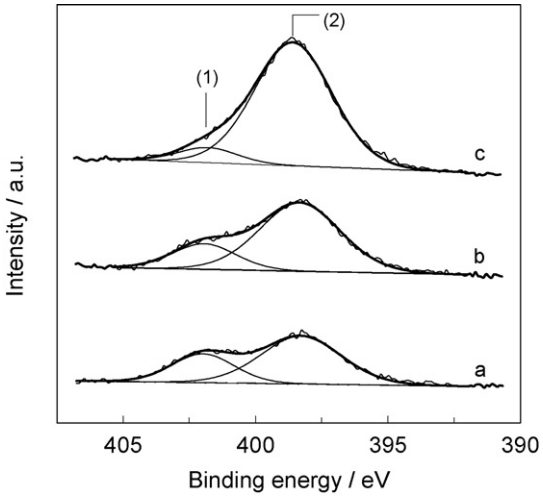

Fig. 11. Part of the XPS spectra of: (a) AA8300; (b) AA8400; (c) AA8500. The mark (1) indicates the N 1s contribution and the mark (2) indicates the Mo $3p_{3/2}$ contribution.

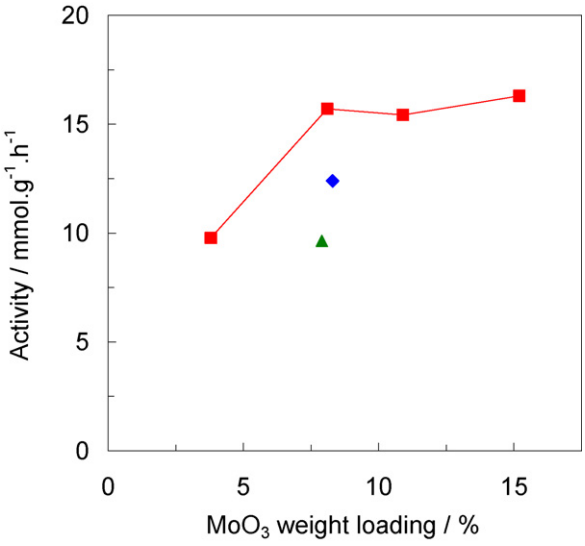

Fig. 12. Maximum specific activity obtained with: (▲) AA8300; (♦) AA8400; (■) AA*x*500 as a function of the MoO_3 weight loading.

[37], a slow deactivation takes place. Here, as all catalysts follow the same trend, it was decided to compare the samples in terms of "maximum specific activity" (Fig. 12). This parameter was arbitrarily defined as the average of the three activity data points taken at 14, 22 and 30 min time-on-stream. This is the period where the activity of the catalysts is the most stable. It appears clearly that increasing the calcination temperature leads to increased catalytic performances. Comparing the catalysts calcined at 500 °C, Fig. 12 shows that the maximum activity first increases significantly when the loading is raised from 4 to 8%. Further increase in the MoO_3 loading does not provoke any significant increase in the performances.

4. Discussion

4.1. Interaction of Mo with the support

The inorganic support onto which the active phase is deposited is sometimes visualized as an inert component of the catalyst having mainly a physical role of carrier of the active phase. Nevertheless, some results indicate that the silica–alumina support is actually reacting chemically with the Mo precursor and interacts strongly with the active phase of the catalyst. In addition, the decisive role of the composition of the support was demonstrated previously [6,7], showing again that the interaction between Mo species and the support during the impregnation step deserves being addressed.

Several works (for example from the group of Weckhuysen and co-workers [21,38] and the group of Che and co-workers [35]) have demonstrated that oxomolybdenum species interact strongly with an alumina support, which can lead to an uneven distribution of Mo at the surface of the support. It was explained for example that the electrostatic interaction between the heptamolybdate anions in solution and the surface of the support favours a preferential adsorption of Mo at the external surface of the particles of the support [21]. Here also, the heptamolybdate species are the main species in the impregnation solution (Fig. 1) and such interactions can be expected in the present case too, possibly resulting in an uneven distribution of the Mo phase.

The ^{27}Al MAS-NMR investigations showed that the environment of Al atoms changed after impregnation with ammonium heptamolybdate. As mentioned in the result part, the attribution of the peak at 15 ppm is a matter of debate. It is sometimes referred to

as a "hydrated form of aluminum molybdate". It is indeed usually detected along with the peak at −14 ppm (related to the $Al_2(MoO_4)_3$ phase) in proportions that depend on the hydration of the sample. Bao et al. have extensively reported the occurrence of this signal in Mo/HBeta-Al_2O_3 metathesis catalysts and have even correlated the build up of aluminum molybdate (hydrated and non-hydrated forms) with a decrease in the metathesis activity of their catalysts [14,39]. Their attribution relies on the work of Edwards and Decanio [40] who provided the tentative formula $[Al(OH)_n(H_2O)_{6-n}]_n(MoO_4)$ with $n = 1$ or 2.

In the late 1990 however, Carrier et al. described the interaction of AHM with alumina during the preparation of MoO_3/Al_2O_3 catalysts and proposed a more precise attribution of the peak at 15 ppm [35]. This work demonstrated the formation of an Anderson-type heteropolymolybdate $[Al(OH)_6Mo_6O_{18}]^{3-}$ during the impregnation step. This species (abbreviated to $[AlMo_6]$) forms during the impregnation step by complexation of dissolved Al^{3+} cations with oxomolybdenum species in solution. $[AlMo_6]$ gives a sharp NMR signal at 15 ppm. It was also observed by Plazenet et al. in the preparation of zeolite-supported MoO_3 catalysts [41]. In fact the calcination of $[AlMo_6]$ yields both MoO_3 and $Al_2(MoO_4)_3$ following the decomposition reaction (1) and the rehydration of such calcined catalyst can lead to partial reconversion of $Al_2(MoO_4)_3$ to $[Al(OH)_6Mo_6O_{18}]^{3-}$ following equation (2) [42]. Nowadays, such Al NMR peak at ca. 15 ppm is more frequently attributed to the presence of the $[AlMo_6]$ species [36,43,44].

$$2\,H_3[Al(OH)_6Mo_6O_{18}] \rightarrow 9MoO_3 + Al_2(MoO_4)_3 + 9H_2O \quad (1)$$

$$2Al_2(MoO_4)_3 + 24H_2O \rightarrow [Al(OH)_6Mo_6O_{18}]^{3-} + 3[Al(H_2O)_6]^{3+} + 6OH^- \quad (2)$$

In any case, NMR results show that the impregnation of the silica–alumina support with ammonium heptamolybdate implies strong interactions between Mo species and Al atoms from the support. The interaction is strong enough to extract Al atoms from their initial environment, to form a new mixed compound. Calcination then affects again the nature and proportions of Mo species at the surface of the catalyst.

4.2. Effect of the calcination temperature

4.2.1. Nature of Mo species

The thermal treatment influenced markedly the crystallinity of the 8% loaded catalysts. Higher calcination temperature obviously favoured the sintering of the MoO_3 phase to form crystals. As far as Raman measurements are concerned, the formation of MoO_3 crystals is also confirmed for the catalysts calcined at higher temperature. The Raman background is unfortunately too intense to observe the signals related to amorphous and dispersed MoO_x species in details. These species indeed have a low Raman cross section. The observation of the band at 950 cm^{-1} however is clear evidence that part of the MoO_x phase is present in the form of surface polymolybdates.

The main observation made from ^{27}Al MAS-NMR measurements is that an aluminium polymolybdate phase (hexamolybdoaluminate denoted $[AlMo_6]$) appears after impregnation of AHM. Calcination provokes the partial conversion of this phase to an aluminum molybdate phase $Al_2(MoO_4)_3$ (detected in NMR at −14 ppm) and to crystalline MoO_3 (detected in XRD and Raman). At first sight, XRD diffractograms do not totally rule out the presence of crystalline $Al_2(MoO_4)_3$ since the main diffraction line of this phase (23.4° following JCPDS 20-0034) falls very close to one of the main diffraction line of MoO_3 (23.3°). However, the other smaller peaks of $Al_2(MoO_4)_3$ are not detected (26.3°, 22.2°, 21.0°, 28.1°, etc.). In addition, the presence of the other minor diffraction lines related to MoO_3 (12.7°, 33.7°, 39.0°, etc.) and their relative intensities attest that the only crystalline phase detected is MoO_3. Accordingly, the aluminium molybdate phase is either amorphous or present in the form of very small crystallites. The $[AlMo_6]$ phase is not detected in XRD either (a reference spectra of $[AlMo_6]$ is reported by Carrier et al. [45]).

4.2.2. Location of the Mo phase

The textural properties of AA8 catalysts are not affected by calcination temperature (Table 1, Fig. 4). Only a limited decrease in pore volume is observed for the AA8 catalysts as compared to the bare support but this is simply attributable to the addition of non-porous MoO_3. The shape of the pore size distribution curves and the mean pore diameters are not affected by impregnation with 8 wt.% of MoO_3. These two observations suggest that the MoO_3 deposit is rather located at the external surface of the support particles and does not fill the interior of the pores. In addition, the estimation of the crystals size via the Debye–Scherrer equation supports the idea that the MoO_3 crystals formed on the 500 °C-treated sample are located at the outer surface of the support particles. Indeed, the average crystal size (35–40 nm) is much higher than the average pore size (ca. 5 nm), implying that such crystals cannot be accommodated inside the pores of the support. In XPS the concentration of Mo was higher at the surface of the catalysts calcined at higher temperature. As the calcination temperature increases, MoO_3 crystals form at the outer surface of the support particles (and not inside the pores), and the Mo surface concentration detected by XPS gets higher.

It is well-known that the wetting of the support by Mo oxide is promoted by high temperature treatments [12]. The tendency of MoO_3 to spread over the surface of another oxide under the effect of a thermal treatment is even used in the preparation of supported MoO_3 catalysts (the technique is known as "thermal spreading" [11,46] and has already been used to prepare MoO_3-based metathesis catalysts [19,47]). So two opposite phenomena take place during calcination: (i) sintering to bulky MoO_3 crystals at the outer surface of the particles (when the temperature, the Mo surface density and the number of nucleation points are high) and (ii) spreading of Mo atoms on the whole available support surface. The Mo deposit that forms on the support after evaporation of water is likely poorly dispersed, due to the interaction of heptamolybdate ions with the external surface of the support [21]. This agglomerated but amorphous phase – formed by adsorbed heptamolybdate species and $[AlMo_6]$ – appears to be only weakly perturbed by calcination at 300 °C. Treatments at higher temperature on the other hand change the morphology of the deposit. During that process, part of the Mo atoms would crystallize into bulk MoO_3 or convert into $Al_2(MoO_4)_3$. The other Mo atoms (presumably those that are not included in $[AlMo_6]$ or those that are not enough agglomerated to nucleate and sinter into MoO_3 crystals) could be further dispersed under the effect of temperature.

4.2.3. Correlation with metathesis activity

Overall, increasing the calcination temperature led to a marked increase in catalytic activity. This crucial effect of calcination temperature may appear surprising considering the activation step at 550 °C under nitrogen that all catalysts undergo before being tested. While this activation could have been expected to level off the properties of similar catalysts, our results show that the "preparation history" of the catalysts is crucial.

As discussed above, higher calcination temperature led to higher proportion of crystalline MoO_3. The higher activity of the catalysts treated at higher temperature thus appears in contradiction with reports that indicate the inactivity of crystalline MoO_3 in the metathesis reaction [19,48]. However, only crystalline MoO_3

is detected in XRD. With this technique, the quantitative description of amorphous species (which presumably yield active centres) is impossible. Also, it should be recalled that only a very small fraction of the Mo atoms present in the catalyst are thought to turn into active centres [9]. So, even if the tendency of Mo atoms to form crystals clearly increases when the calcination temperature is enhanced, it may be put forward that the nature and proportion of remaining amorphous species are also (beneficially) affected by high calcination temperature, thereby influencing positively the activity of the catalysts.

Another impact that the calcination temperature can have on the amorphous Mo species is linked to the chemical environment of the Mo atoms. The environment of Al atoms as studied by MAS-NMR indirectly gives indications on the interaction of these atoms with Mo atoms. It seems that mainly Al_{OCT} and Al_{PEN} atoms are extracted from their natural positions in silica–alumina and participate in the interaction with Mo. In the dried catalyst, these two components are indeed reduced and a large peak of [$AlMo_6$] is detected. Calcination provoked the quasi-restoration of each species. Calcining the catalyst at higher temperature provokes the more complete restoration of the Al_{OCT} and Al_{PEN} contributions. In parallel, the contribution of [$AlMo_6$] becomes smaller and when the calcination temperature is high, the $Al_2(MoO_4)_3$ phase appears. Both phases were however reported to be inactive for the metathesis reaction [8,14,39]. So, the positive effect brought by higher calcination temperature can likely not be accounted by the formation of these mixed phases.

It was shown (Fig. 11) that the removal of ammonium moieties is not completed after the 2 h of calcination. At low calcination temperature the amount of remaining N is high. On the 300 °C-treated sample, the N/Mo atomic ratio is even higher than for pure AHM. This can be explained by the strong interaction between the $Mo_7O_{24}^{6-}$ species and the surface of the support: during the impregnation, the Mo clusters are first fixed on the support, while the counter cations are still in the impregnation solution. Ammonium ions are subsequently deposited on top of the Mo deposit at the end of the evaporation step. This coverage might be the cause of the lower activity of the samples calcined at low temperature.

4.3. Effect of the MoO_3 loading

4.3.1. Nature and location of Mo species

When the thermal treatment was kept constant, a clear increase in the intensity of the crystalline MoO_3 diffraction lines was observed with increasing loading. This suggests that the proportion Mo atoms involved in crystals is rising when the MoO_3 loading increases. In parallel, the proportion of Mo detected in XPS increases in a linear way (Fig. 10). Also, regardless of the Mo loading, the porosity of the support was not significantly affected. These observations indicate that the MoO_3 crystals build up at the outer surface of the support. The environment of Al atoms appears only slightly affected by changes in the MoO_3 loading. The main modification concerns the signal of the aluminium molybdate phase which increases with increasing loading.

4.3.2. Correlation with metathesis activity

The specific activity was shown to increase from about 10 to about 16 mmol g^{-1} h^{-1} when the MoO_3 loading rises from 4 to 8 wt.%. A levelling off in the performances of the catalysts was observed above 8 wt.% MoO_3 loading (Fig. 12). This rupture in the activity-loading curve corresponds to the loading (8 wt.%) at which MoO_3 crystals start to be detected in XRD (Fig. 6). The $Al_2(MoO_4)_3$ phase also builds up noticeably when the loading is increased above 8 wt.% of MoO_3 (Fig. 9).

Such limit is classically observed with supported MoO_3 catalysts [13]. Liu et al. [15] reported an optimum of loading around 5–9 wt.% for MoO_3 supported on a HBeta zeolite support in the cross-metathesis of ethene and 2-butene to propene. Above this loading, the performance decreases. Handzlik et al. observed higher specific activity for the MoO_3/SiO_2–Al_2O_3 catalysts with 4–7 wt.% of MoO_3 [7]. Grunert et al., when using activation conditions similar to ours (550 °C under Ar), found the metathesis activity of MoO_3/Al_2O_3 catalysts to level off in the 7–13 wt.% MoO_3 range [49]. Such limitation is sometimes interpreted on the basis of the number of available acid sites at the surface of the support [7]. As demonstrated in a recent work, the Al content in the support and its corresponding surface acidity have a marked influence on the metathesis activity of MoO_3/SiO_2–Al_2O_3 formulations [6]. Accordingly, it has been proposed that only Mo species that are deposited on sites with appropriate acidic character yield active metathesis centres [7]. The saturation of those sites with the increasing amount of Mo could be called to explain the plateau observed in Fig. 12. Besides, the limit in terms of activity at high loading can be interpreted on the basis of the formation of inactive agglomerated MoO_x species (polymers or crystals). The characterization data presented here support this analysis. Our interpretation of the activity-loading relationship is that the number of dispersed – potentially active – species does not increase when the loading is increased above 8% because most additional Mo atoms join either the MoO_3 crystals or the aluminium molybdate phase. At this stage it is not possible to discriminate which of these species has the most decisive responsibility in limiting the performances of the MoO_3/SiO_2–Al_2O_3 catalysts.

5. Conclusion

This paper investigated the impact of two important parameters in the preparation of a MoO_3/SiO_2–Al_2O_3 catalyst by wet impregnation of ammonium heptamolybdate: the calcination temperature and the loading. It also shows that the support interacts with Mo species in solution during the impregnation step. In fact a hexamolybdoaluminate phase is formed during impregnation. This species is partly converted upon calcination to MoO_3 crystals and to $Al_2(MoO_4)_3$. Raman spectroscopy shows also that part of the Mo phase is preserved as amorphous surface polymolybdate.

It was shown that the calcination temperature has a marked impact on the activity of the catalysts: samples treated at 500 °C perform better than catalysts treated at 400 °C, themselves being more active than those treated at 300 °C. After calcination at higher temperatures, the amount of Mo oxide at the surface of the support appeared higher (XPS), which is correlated to the build up of MoO_3 crystals at the outer surface of the support. It is suggested that the dispersion of the remaining amorphous species is affected (beneficially) by high calcination temperature. The decomposition of the precursor salt is also more readily achieved.

Increasing the MoO_3 loading from 4 to 8 wt.% increases the metathesis activity of the catalyst. Above 8% however, inactive MoO_3 crystals and an $Al_2(MoO_4)_3$ phase build up preferentially and the performance of the catalyst levels off. As a conclusion, for this kind of systems prepared through the rather classical approach of wet impregnation with ammonium heptamolybdate, overloading should be avoided. Ca. 8% is identified as a limit above which further increase in the loading is useless. Strategies for improving the performances of MoO_3/SiO_2–Al_2O_3 catalysts should be based on the search for better spreading of the active phase on the whole available support surface (including the pores). Impeding the formation of the [$AlMo_6$] heteropolyanion during impregnation also appears to be a relevant approach because this species was shown to convert into inactive MoO_3 crystals and aluminium molybdate.

Acknowledgments

Guy Daelen is acknowledged for having performed the NMR experiments. The authors acknowledge the Université catholique de Louvain and the Fonds National de la Recherche Scientifique (FNRS) of Belgium. D.P. Debecker thanks the FNRS for his research fellow position. The authors from UCL and FUNDP are involved in the "Inanomat" IUAP network sustained by the service public fédéral de programmation politique scientifique (Belgium). The authors from UCL are also involved in the Cost Action D41 sustained by the European Science Foundation and in the European Multifunctional Material Institute (EMMI) built on the basis of the former "FAME" Network of Excellence of the EU 6th FP.

Appendix A. Supplementary data

Supplementary data associated with this article can be found, in the online version, at doi:10.1016/j.cattod.2010.07.026.

References

[1] P.C. Bakala, E. Briot, J.Y. Piquemal, J.M. Bregeault, P. Beaunier, Catal. Commun. 8 (2007) 1447–1451.
[2] J. Handzlik, J. Ogonowski, R. Dula, J. Stoch, E.M. Serwicka, React. Kinet. Catal. Lett. 79 (2003) 135–141.
[3] D.P. Debecker, K. Bouchmella, C. Poleunis, P. Eloy, P. Bertrand, E.M. Gaigneaux, P.H. Mutin, Chem. Mater. 21 (2009) 2817–2824.
[4] J. Handzlik, Surf. Sci. 601 (2007) 2054–2065.
[5] H. Aritani, O. Fukuda, A. Miyaji, S. Hasegawa, Appl. Surf. Sci. 180 (2001) 261–269.
[6] D.P. Debecker, D. Hauwaert, M. Stoyanova, A. Barkschat, U. Rodemerck, E.M. Gaigneaux, Appl. Catal. A (2010), doi:10.1016/j.apcata.2010.06.021, in press.
[7] J. Handzlik, J. Ogonowski, J. Stoch, M. Mikolajczyk, P. Michorczyk, Appl. Catal. A 312 (2006) 213–219.
[8] X. Li, W. Zhang, S. Liu, X. Han, L. Xu, X. Bao, J. Mol. Catal. A 250 (2006) 94–99.
[9] J. Handzlik, J. Ogonowski, Catal. Lett. 88 (2003) 119–122.
[10] J. Handzlik, P. Sautet, J. Phys. Chem. C 112 (2008) 14456–14463.
[11] S. Braun, L.G. Appel, V.L. Camorim, M. Schmal, J. Phys. Chem. B 104 (2000) 6584–6590.
[12] S. Gunther, F. Esch, L. Gregoratti, A. Barinov, M. Kiskinova, E. Taglauer, H. Knozinger, J. Phys. Chem. B 108 (2004) 14223–14231.
[13] K.J. Ivin, J.C. Mol, Olefin Metathesis and Metathesis Polymerization, Academic Press, London, 1997.
[14] X. Li, W. Zhang, S. Liu, L. Xu, X. Han, X. Bao, J. Phys. Chem. C 112 (2008) 5955–5960.
[15] S. Liu, S. Huang, W. Xin, J. Bai, S. Xie, L. Xu, Catal. Today 93–95 (2004) 471–476.
[16] A.N. Startsev, O.V. Klimov, E.A. Khomyakova, J. Catal. 139 (1993) 134–141.
[17] H. Aritani, O. Fukuda, T. Yamamoto, T. Tanaka, S. Imamura, Chem. Lett. (2000) 66–67.
[18] H. Balcar, P. Topka, N. Zilkova, J. Perez-Pariente, J. Cejka, Stud. Surf. Sci. Catal. 156 (2005) 795–802.
[19] P. Topka, H. Balcar, J. Rathousky, N. Zilkova, F. Verpoort, J. Cejka, Micropor. Mesopor. Mater. 96 (2006) 44–54.
[20] U. Rodemerck, P. Ignaszewski, M. Lucas, P. Claus, Chem. Eng. Technol. 23 (2000) 413–416.
[21] J.A. Bergwerff, T. Visser, B.R.G. Leliveld, B.D. Rossenaar, K.P. de Jong, B.M. Weckhuysen, J. Am. Chem. Soc. 126 (2004) 14548–14556.
[22] G. Mestl, T.K.K. Srinivasan, Cat. Rev. Sci. Eng. 40 (1998) 451–570.
[23] M. May, M. Asomoza, T. Lopez, R. Gomez, Chem. Mater. 9 (1997) 2395–2399.
[24] E.J.M. Hensen, D.G. Poduval, P.C.M.M. Magusin, A.E. Coumans, J.A.R. van Veen, J. Catal. 269 (2010) 201–218.
[25] C.L. Thomas, Ind. Eng. Chem. 41 (1949) 2564–2573.
[26] R.C. Hansford, Ind. Eng. Chem. 39 (1947) 849–852.
[27] K.J.D. MacKenzie, J. Temuujin, K. Okada, Thermochim. Acta 327 (1999) 103–108.
[28] T.-H. Chen, K. Houthoofd, P.J. Grobet, Micropor. Mesopor. Mater. 86 (2005) 31–37.
[29] P. Cloos, A.J. Leonard, J.P. Moreau, A. Herbillon, J.J. Fripiat, Clays Clay Miner. 17 (1969) 279–287.
[30] A. Samoson, E. Lippmaa, G. Engelhardt, U. Lohse, H.G. Jerschkewitz, Chem. Phys. Lett. 134 (1987) 589–592.
[31] Z. Vít, O. Solcová, Micropor. Mesopor. Mater. 96 (2006) 197–204.
[32] J.P. Gilson, G.C. Edwards, A.W. Peters, K. Rajagopalan, R.F. Wormsbecher, T.G. Roberie, M.P. Shatlock, J. Chem. Soc. Chem. Commun. (1987) 91–92.
[33] L. Kellberg, M. Linsten, H.J. Jakobsen, Chem. Phys. Lett. 182 (1991) 120–126.
[34] M.F. Williams, B. Fonfé, C. Sievers, A. Abraham, J.A. van Bokhoven, A. Jentys, J.A.R. van Veen, J.A. Lercher, J. Catal. 251 (2007) 485–496.
[35] X. Carrier, J.F. Lambert, M. Che, J. Am. Chem. Soc. 119 (1997) 10137–10146.
[36] T. Klimova, J. Reyes, O. Gutiérrez, L. Lizama, Appl. Catal. A 335 (2008) 159–171.
[37] X.J. Li, W.P. Zhang, X. Li, S.L. Liu, H.J. Huang, X.W. Han, L.Y. Xu, X.H. Bao, J. Phys. Chem. C 113 (2009) 8228–8233.
[38] J.A. Bergwerff, M. Jansen, B.G. Leliveld, T. Visser, K.P. de Jong, B.M. Weckhuysen, J. Catal. 243 (2006) 292–302.
[39] X. Li, W. Zhang, S. Liu, L. Xu, X. Han, X. Bao, J. Catal. 250 (2007) 55–66.
[40] J.C. Edwards, E.C. Decanio, Catal. Lett. 19 (1993) 121–130.
[41] G. Plazenet, E. Payen, J. Lynch, B. Rebours, J. Phys. Chem. B 106 (2002) 7013–7028.
[42] X. Carrier, M. Che, Appl. Catal. A 253 (2003) 317–320.
[43] A. Sampieri, S. Pronier, S. Brunet, X. Carrier, C. Louis, J. Blanchard, K. Fajerwerg, M. Breysse, Micropor. Mesopor. Mater. 130 (2010) 130–141.
[44] G. Macías, J. Ramírez, A. Gutiérrez-Alejandre, R. Cuevas, Catal. Today 133–135 (2008) 261–266.
[45] X. Carrier, E. Marceau, M. Che, Pure Appl. Chem. 78 (2006) 1039–1055.
[46] F.C. Jentoft, H. Schmelz, H. Knözinger, Appl. Catal. A 161 (1997) 167–182.
[47] D.P. Debecker, M. Stoyanova, U. Rodemerck, E.M. Gaigneaux, Stud. Surf. Sci. Catal. 175 (2010) 581–585.
[48] B. Zhang, N. Liu, Q. Lin, D. Jin, J. Mol. Catal. 65 (1991) 15–28.
[49] W. Grunert, A.Y. Stakheev, R. Feldhaus, K. Anders, E.S. Shpiro, K.M. Minachev, J. Catal. 135 (1992) 287–299.